Selective Inhibition of Autotaxin is Efficacious in Mouse Models of Liver Fibrosis

Gretchen Bain, Kristen E. Shannon, Fei Huang , Janice Darlington, Lance Goulet, Patricia Prodanovich, Gina L. Ma, Angelina M. Santini, Adam J. Stein, Dave Lonergan, Christopher D. King, Imelda Calderon, Andiliy Lai, John H. Hutchinson and Jilly F. Evans

Journal of Pharmacology and Experimental Therapeutics

Supplementary Table 1. % Inhibition of ENPP Family Proteins by 10 µM PAT-505.

	ENPP1	ENPP3	ENPP6	ENPP7
% Inhibition	4.9	6.8	-6.8	0.1

Supplementary Table 2. Effect of PAT-505 on PPARγ ligand-dependent coactivator recruitment.

Assay Mode	Concentration of PAT-505		
	100 µM	30 µM	10 µM
% inhibition (antagonism)	123 ± 9 (n=3)	73 ± 6 (n=3)	62 ± 8 (n=3)
% activation (agonism)	ND	-8.2	-2.6

ND = not done; % inhibition represents the average ± SD of three independent experiments.

Selective Inhibition of Autotaxin is Efficacious in Mouse Models of Liver Fibrosis

Gretchen Bain, Kristen E. Shannon, Fei Huang , Janice Darlington, Lance Goulet, Patricia Prodanovich, Gina L. Ma, Angelina M. Santini, Adam J. Stein, Dave Lonergan, Christopher D. King, Imelda Calderon, Andiliy Lai, John H. Hutchinson and Jilly F. Evans

Journal of Pharmacology and Experimental Therapeutics

Supplementary Figure 1

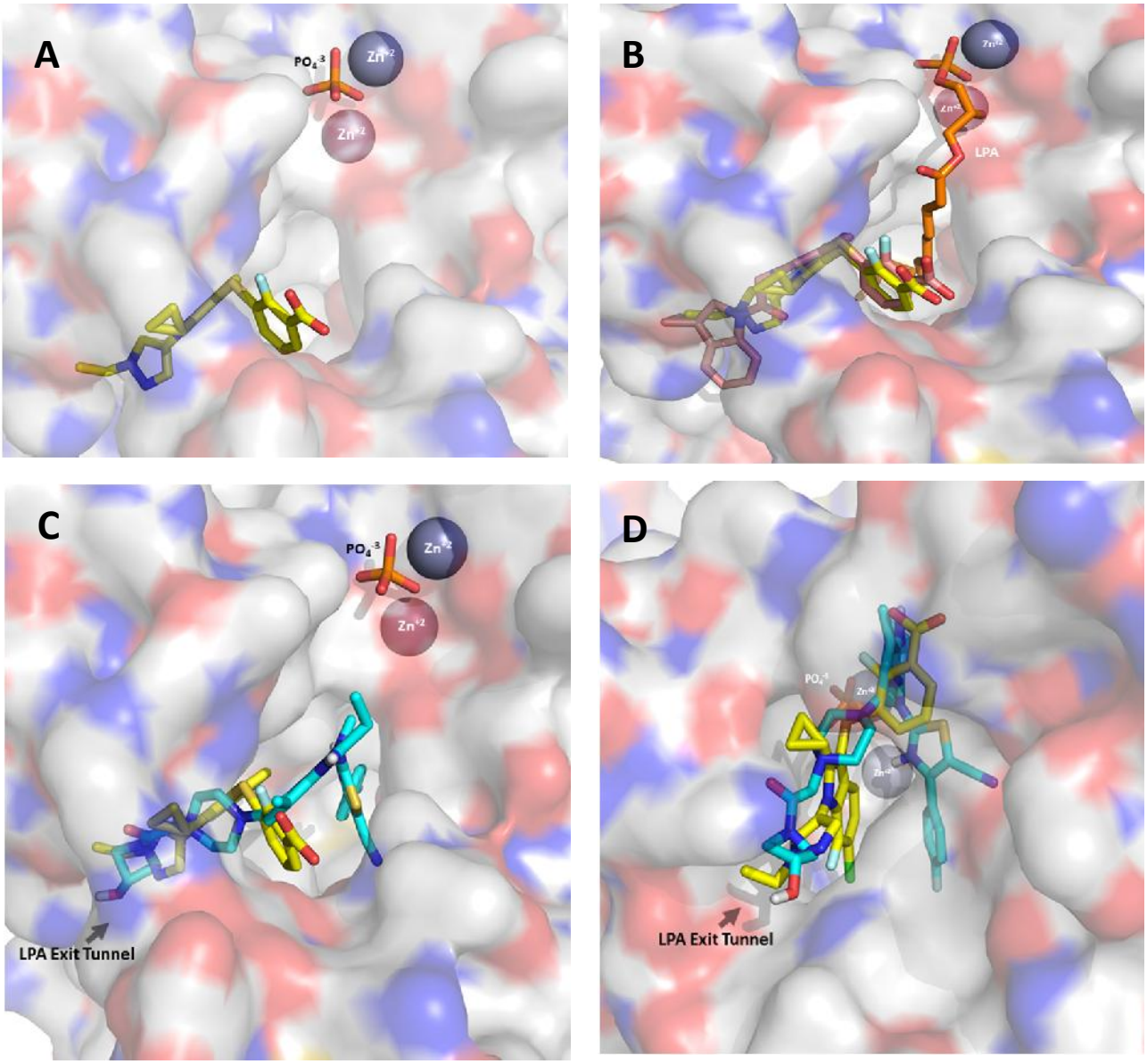

Supplementary Fig. 1. Crystal structure of human ATX bound to PAT-505, PAT-347 and GLPG. (A) Crystal structure of PAT-505 (yellow) bound to human ATX in an allosteric site adjacent to the catalytic site. The zinc coordination site in the catalytic domain is show by the large grey spheres. Also shown is a phosphate ion (orange), a mimic of the phosphate portion of LPA. (B) Overlay of PAT-505 (yellow) with PAT-347 (salmon) in the non-competitive site. LPA (orange) from the PAT-347 crystal is bound to Zn+2 in the active site (C) Overlay of PAT-505 (yellow) with the docked GLPG1690 (cyan). (D) Overlay from panel C rotated 90˚ showing how the GLPG1690 (cyan) thiazol-phenyl group sits in the LPA binding site.

Selective Inhibition of Autotaxin is Efficacious in Mouse Models of Liver Fibrosis

Gretchen Bain, Kristen E. Shannon, Fei Huang , Janice Darlington, Lance Goulet, Patricia Prodanovich, Gina L. Ma, Angelina M. Santini, Adam J. Stein, Dave Lonergan, Christopher D. King, Imelda Calderon, Andiliy Lai, John H. Hutchinson and Jilly F. Evans

Journal of Pharmacology and Experimental Therapeutics

Supplementary Figure 2

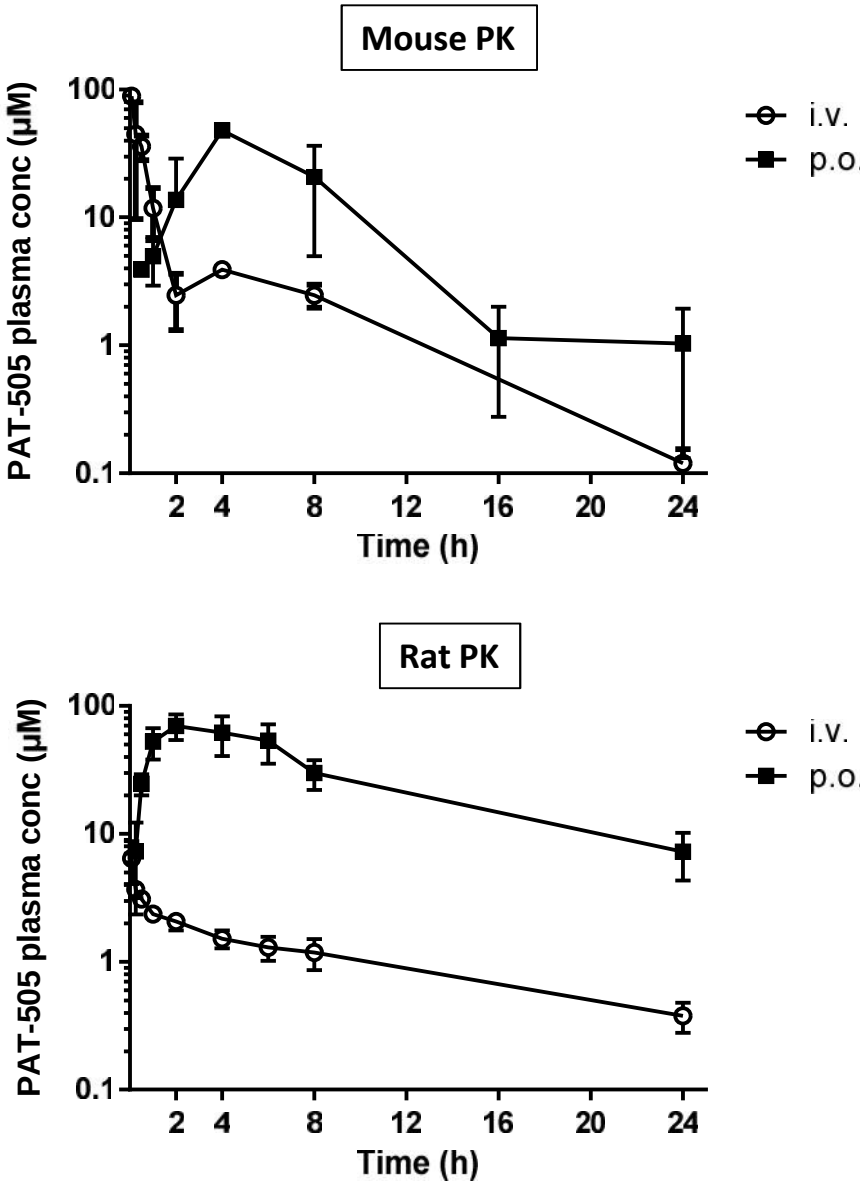

Supplementary Fig. 2. Pharmacokinetic profile of PAT-505. Plasma concentrations of PAT-505 at various times after a single intravenous (i.v.) or oral (p.o.) dose in C57Bl/6 mice or Sprague-Dawley rats. Plotted is the mean plasma concentration ± SD from three different animals.

Selective Inhibition of Autotaxin is Efficacious in Mouse Models of Liver Fibrosis

Gretchen Bain, Kristen E. Shannon, Fei Huang , Janice Darlington, Lance Goulet, Patricia Prodanovich, Gina L. Ma, Angelina M. Santini, Adam J. Stein, Dave Lonergan, Christopher D. King, Imelda Calderon, Andiliy Lai, John H. Hutchinson and Jilly F. Evans

Journal of Pharmacology and Experimental Therapeutics

Supplementary Figure 3

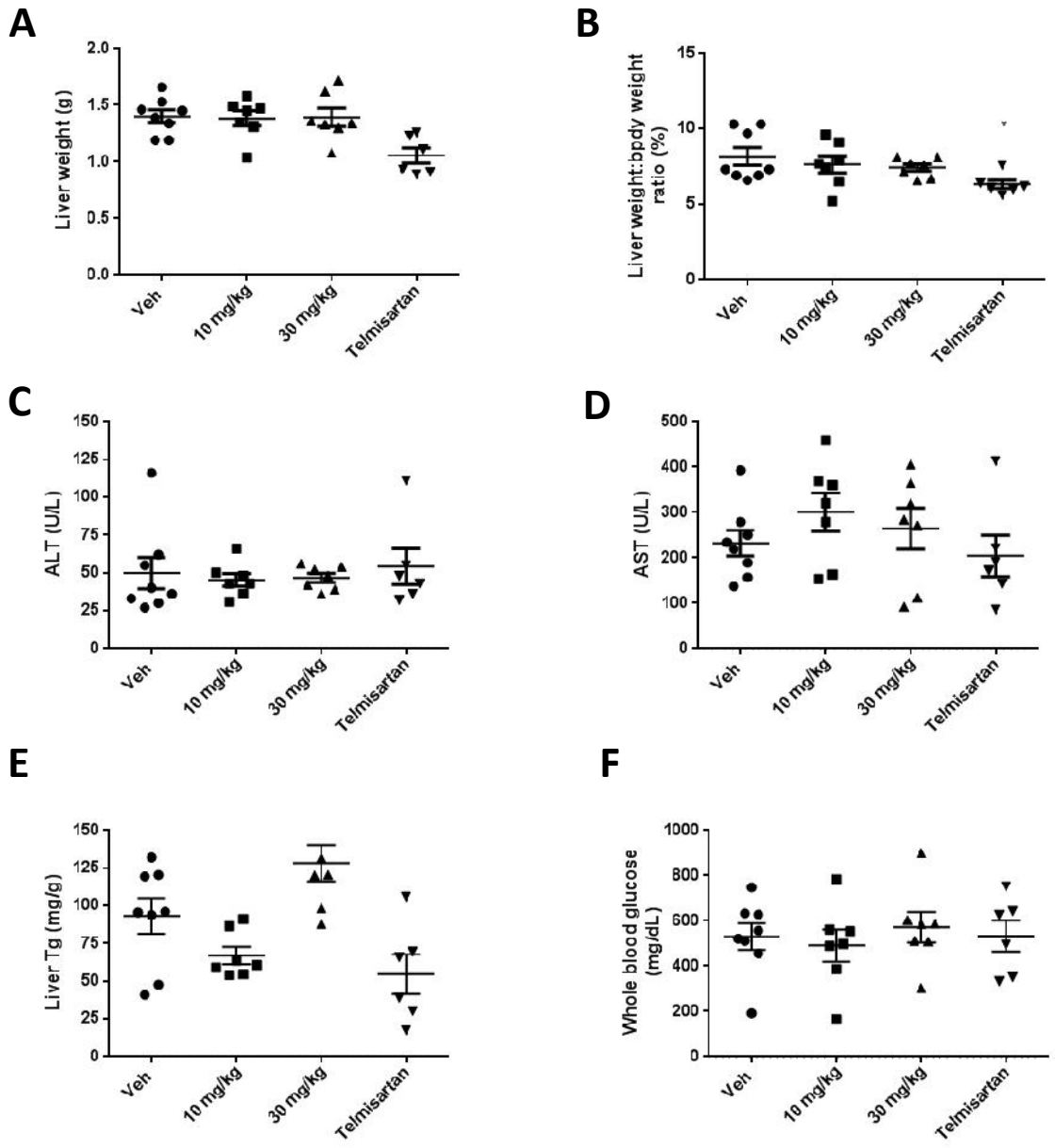

Supplementary Fig. 3. Effect of 10 or 30 mg/kg PAT-505 treatment vs. telemisartan on several parameters in the mouse STAM™ NASH model. Liver weight (A), liver weight:body weight ratio (B), serum ALT (C), serum AST (D), liver triglycerides (E) and whole blood glucose (F) determined at the end of the 12 week study. Plotted are the individual values for each animal with the mean ± SEM indicated.

Selective Inhibition of Autotaxin is Efficacious in Mouse Models of Liver Fibrosis

Gretchen Bain, Kristen E. Shannon, Fei Huang , Janice Darlington, Lance Goulet, Patricia Prodanovich, Gina L. Ma, Angelina M. Santini, Adam J. Stein, Dave Lonergan, Christopher D. King, Imelda Calderon, Andiliy Lai, John H. Hutchinson and Jilly F. Evans

Journal of Pharmacology and Experimental Therapeutics

Supplementary Figure 4

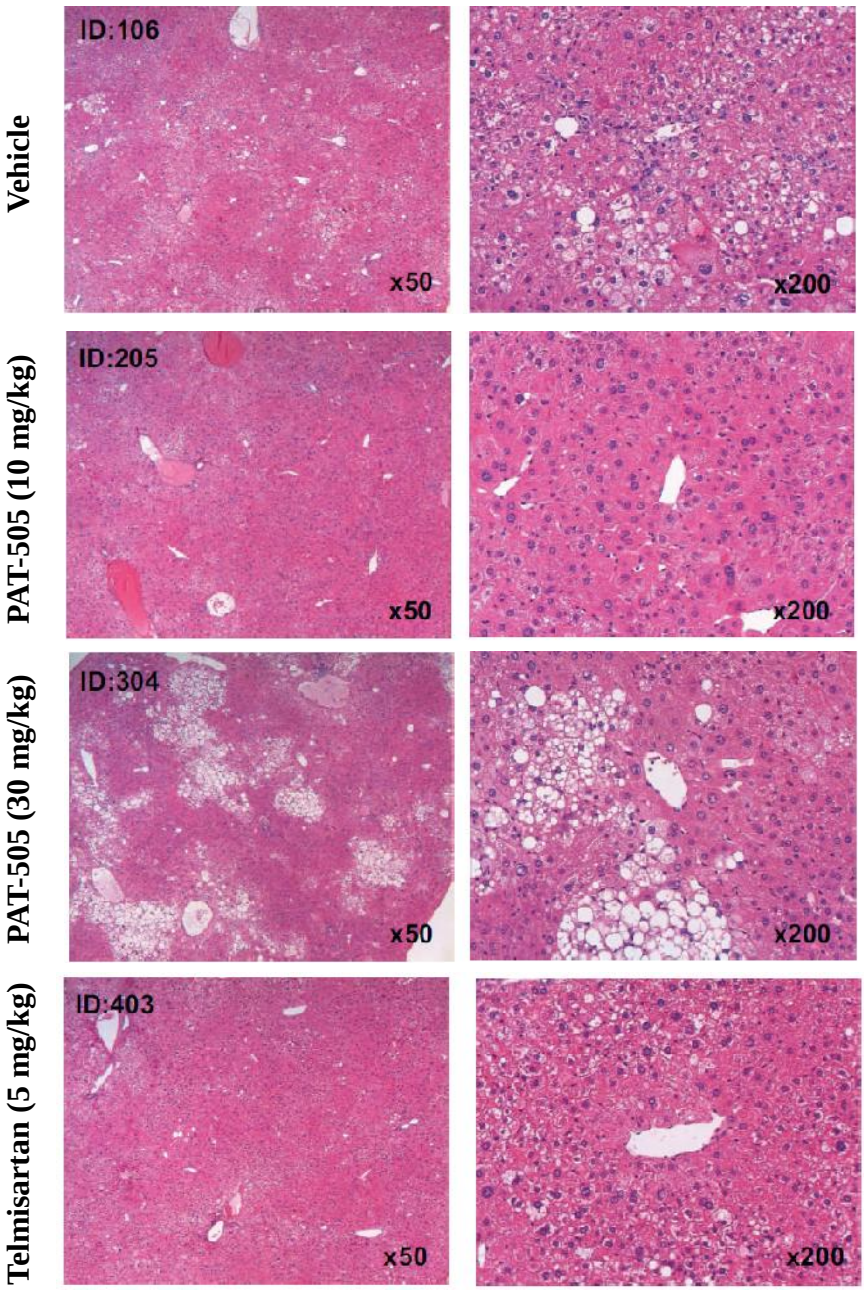

Supplementary Fig. 4. Representative H&E stained liver sections from the mouse STAM™ NASH model. Left panel images are 50X magnification and right panel images are 200X magnification.

Selective Inhibition of Autotaxin is Efficacious in Mouse Models of Liver Fibrosis

Gretchen Bain, Kristen E. Shannon, Fei Huang , Janice Darlington, Lance Goulet, Patricia Prodanovich, Gina L. Ma, Angelina M. Santini, Adam J. Stein, Dave Lonergan, Christopher D. King, Imelda Calderon, Andiliy Lai, John H. Hutchinson and Jilly F. Evans

Journal of Pharmacology and Experimental Therapeutics

Supplementary Figure 5

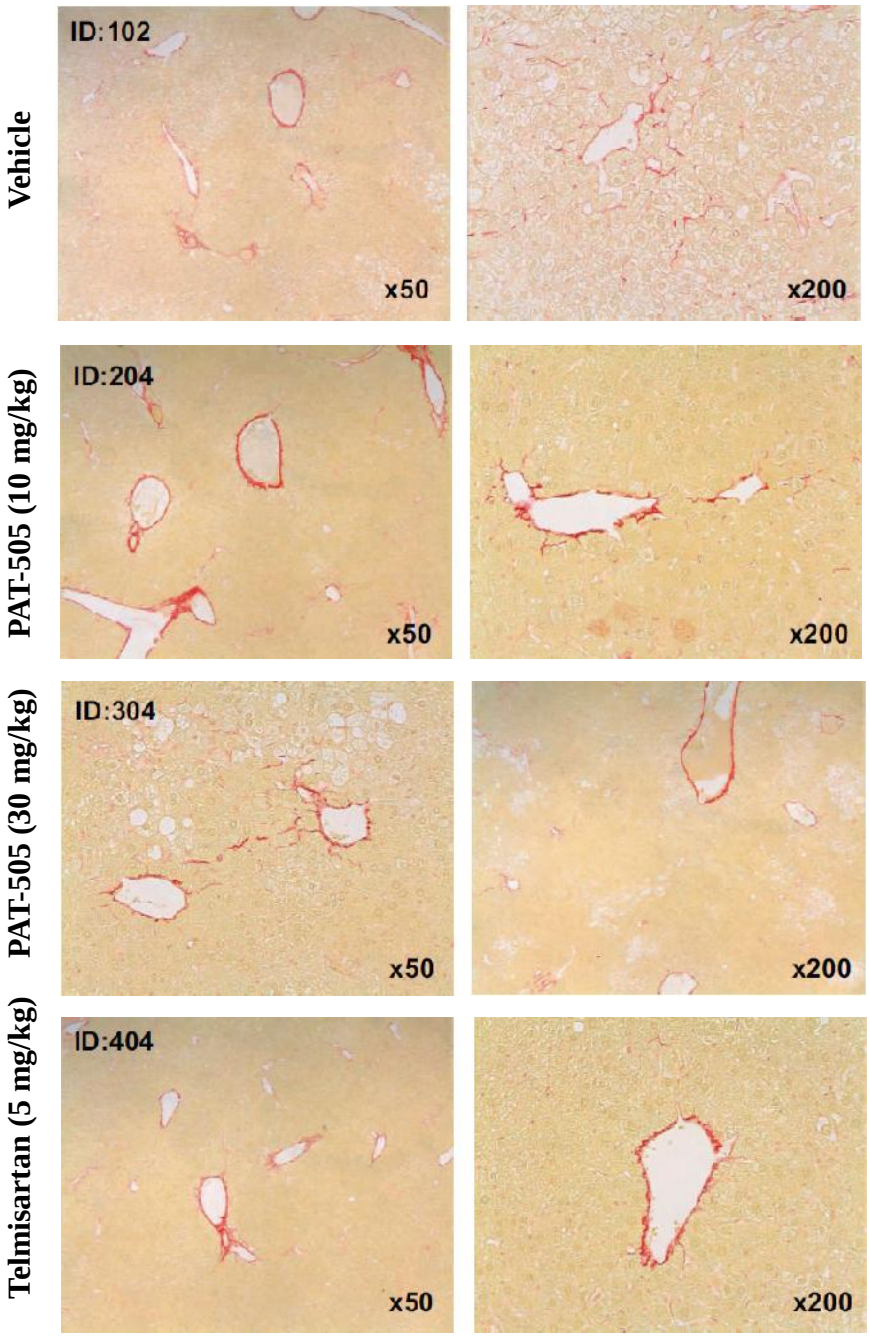

Supplementary Fig. 5. Representative PSR stained liver sections from the mouse STAM™ NASH model. Left panel images are 50X magnification and right panel images are 200X magnification.

Selective Inhibition of Autotaxin is Efficacious in Mouse Models of Liver Fibrosis

Gretchen Bain, Kristen E. Shannon, Fei Huang , Janice Darlington, Lance Goulet, Patricia Prodanovich, Gina L. Ma, Angelina M. Santini, Adam J. Stein, Dave Lonergan, Christopher D. King, Imelda Calderon, Andiliy Lai, John H. Hutchinson and Jilly F. Evans

Journal of Pharmacology and Experimental Therapeutics

Supplementary Figure 6

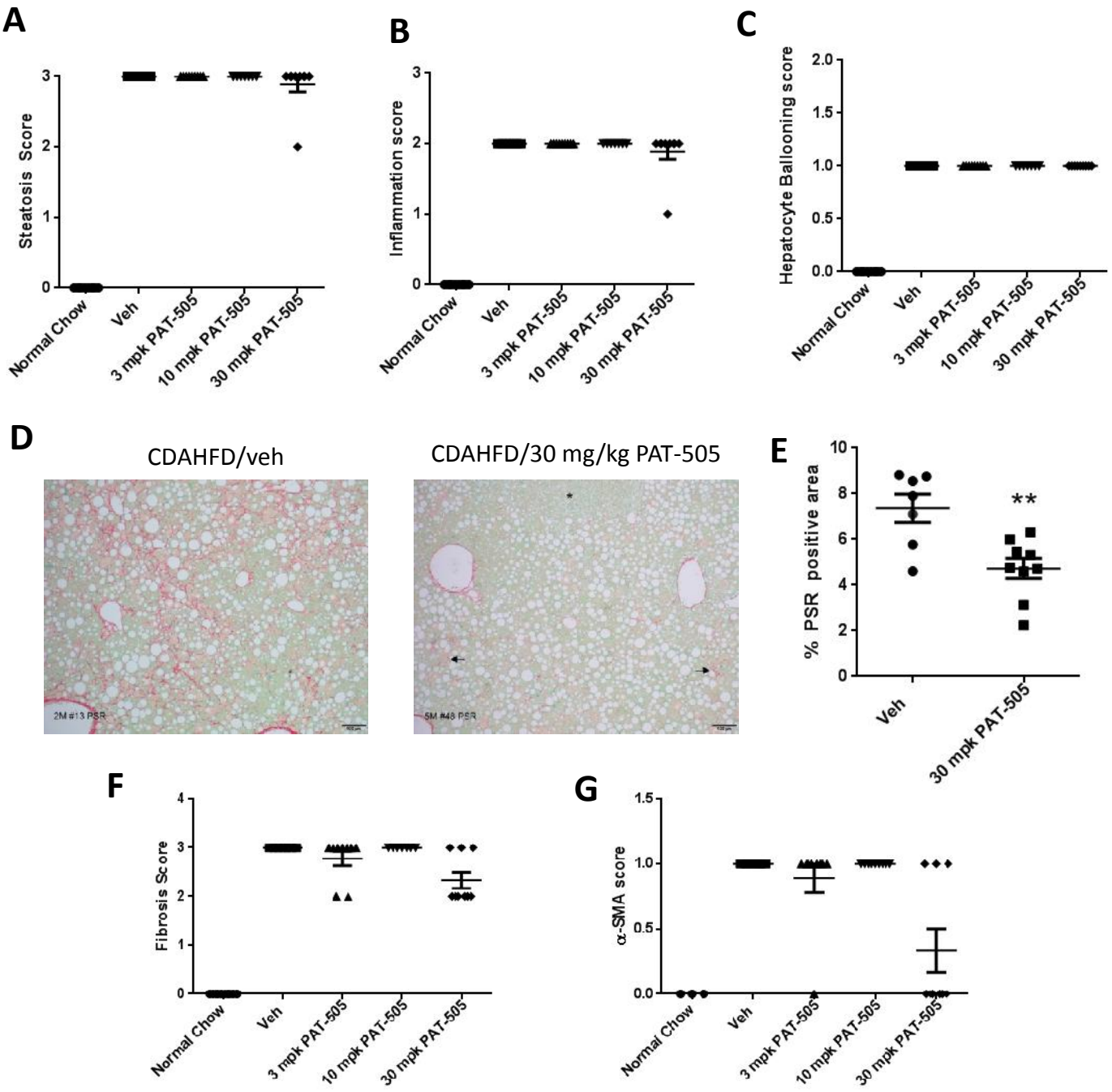

Supplementary Fig. 6. Effect of PAT-505 treatment on hepatic steatosis, inflammation, and fibrosis in the first mouse CDAHFD study. Scores for severity of steatosis (A), lobular inflammation (B) and hepatocyte ballooning (C). (D) Representative PSR stained liver sections from a vehicle and PAT-505 treated CDAHFD animal and (E) quantitation of the percent PSR positive area . Scores for severity of fibrosis (F) and α-SMA immunoreactivity (G). Plotted are the individual values for each animal with the mean ± SEM indicated.

Selective Inhibition of Autotaxin is Efficacious in Mouse Models of Liver Fibrosis

Gretchen Bain, Kristen E. Shannon, Fei Huang , Janice Darlington, Lance Goulet, Patricia Prodanovich, Gina L. Ma, Angelina M. Santini, Adam J. Stein, Dave Lonergan, Christopher D. King, Imelda Calderon, Andiliy Lai, John H. Hutchinson and Jilly F. Evans

Journal of Pharmacology and Experimental Therapeutics

Supplementary Figure 7

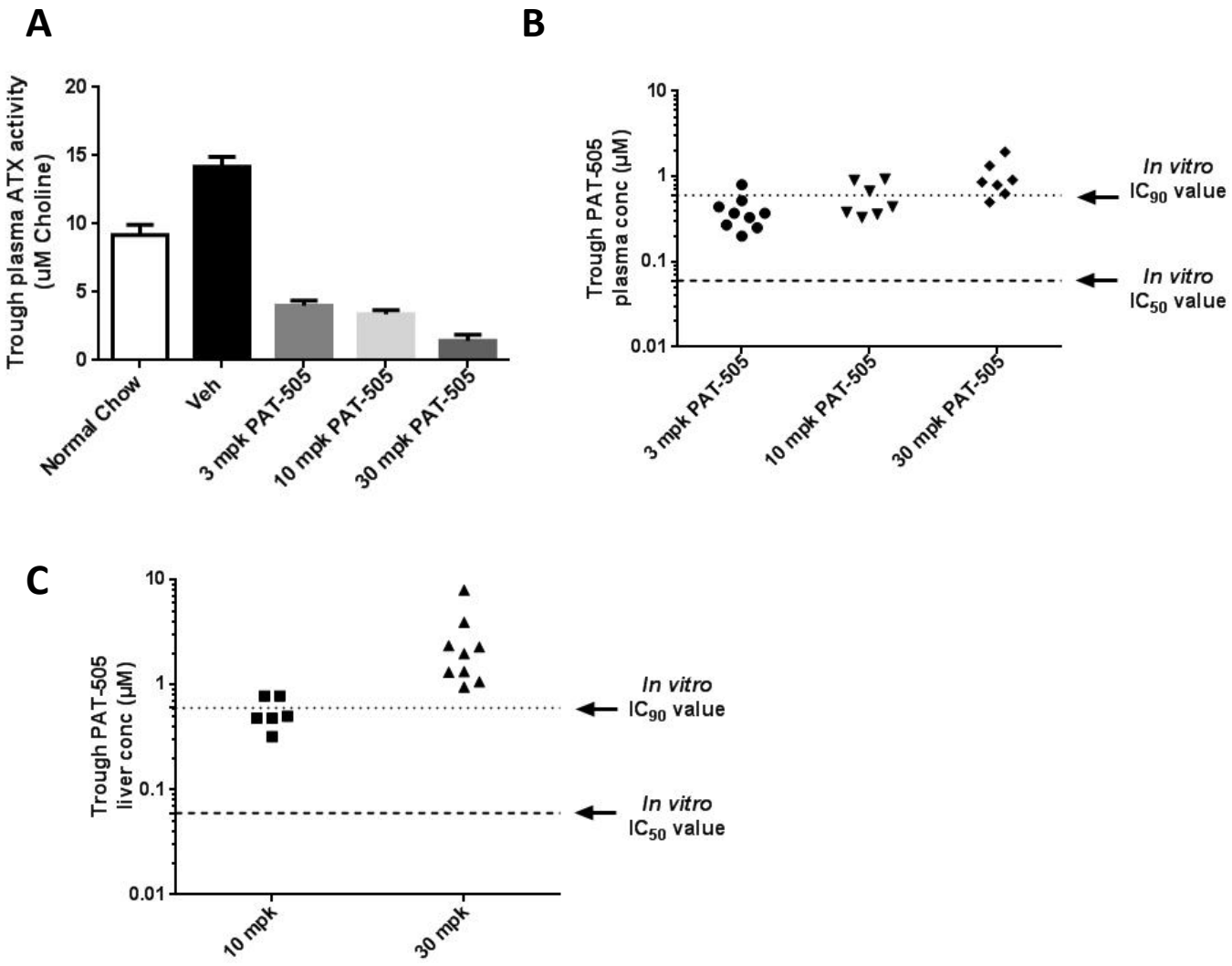

Supplementary Fig. 7. ATX activity and drug concentrations from the first CDAHFD study. (A) Average trough plasma ATX activity ± SEM and (B) trough plasma and (C) trough liver PAT-505 concentrations from animals in the CDAHFD study. For (B) and (C), shown are individual values from each animal and dotted lines which represent the average IC_{50} and IC_{90} values from the *in vitro* mouse plasma assay.

Selective Inhibition of Autotaxin is Efficacious in Mouse Models of Liver Fibrosis

Gretchen Bain, Kristen E. Shannon, Fei Huang , Janice Darlington, Lance Goulet, Patricia Prodanovich, Gina L. Ma, Angelina M. Santini, Adam J. Stein, Dave Lonergan, Christopher D. King, Imelda Calderon, Andiliy Lai, John H. Hutchinson and Jilly F. Evans

Journal of Pharmacology and Experimental Therapeutics

Supplementary Figure 8

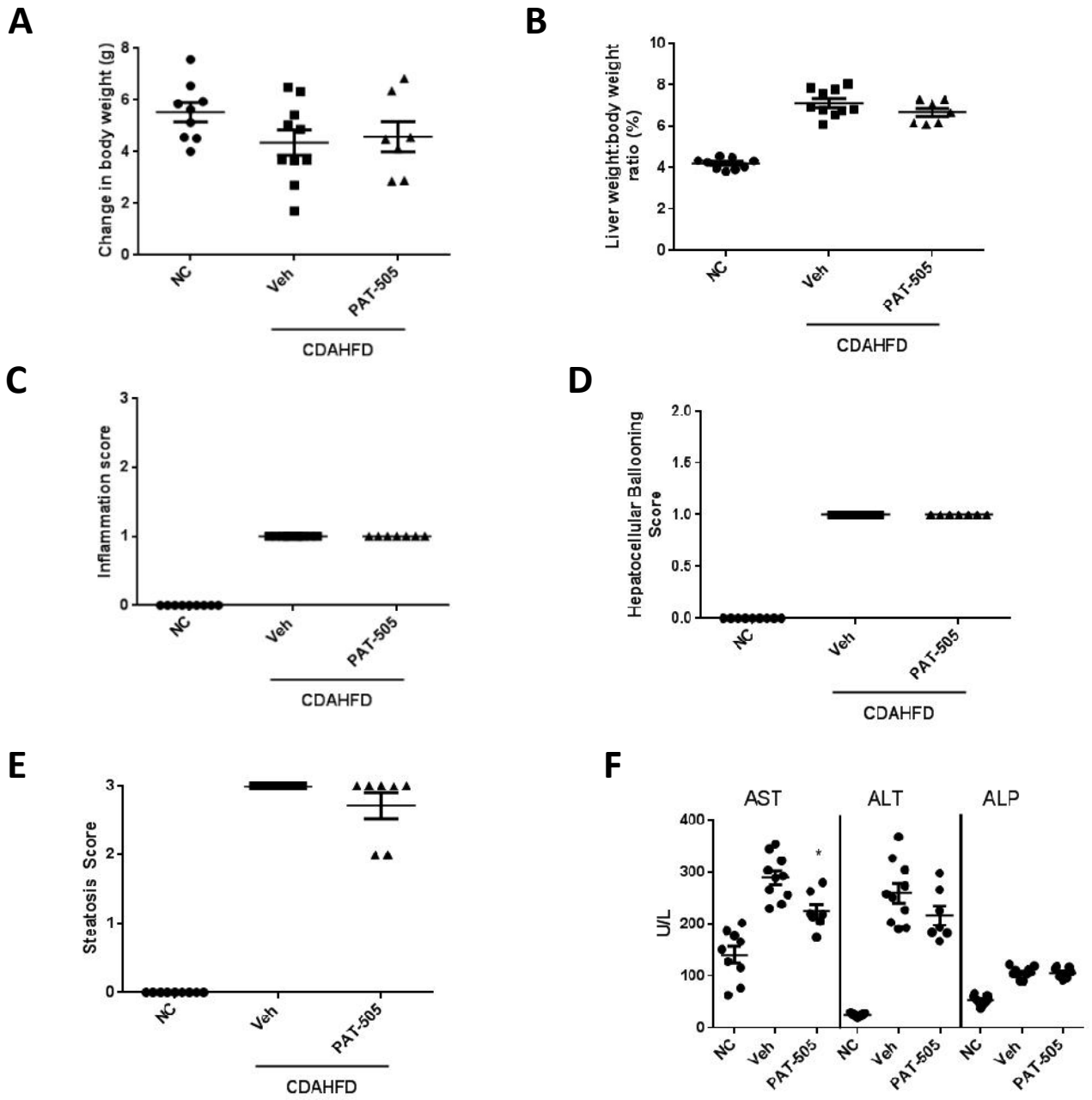

Supplementary Fig. 8. Effect of PAT-505 treatment on several parameters in the second mouse CDAHFD study. Change in body weight (A), liver weight:body weight ratio (B) and scores for severity of lobular inflammation (C), hepatocyte ballooning (D) and steatosis (E). (F) Serum liver enzymes. Plotted are the individual values for each animal with the mean ± SEM indicated.